Invar® oxidation in CO$_2$

Kinetics and mechanism of formation of a wüstite layer

S. Menecier · S. Valette · P. Denoirjean ·
P. Lefort

Abstract In this article, corrosion of Invar® in a static carbon dioxide atmosphere $2 \times 10^4 \leq P_{CO_2} \leq 10^5$ Pa has been studied between 1163 and 1263 K. At the beginning, after a short initial deceleration for weight gains $\Delta m/S$ <0.5 mg cm^{-2}, oxidation kinetics were linear up to weight gains of about 4.0 mg cm^{-2}, and only wüstite Fe$_{1-x}$O was formed with a constant rate r (mg cm^{-2} s^{-1}) $r = \frac{d\left(\frac{\Delta m}{S}\right)}{dt} = 0.41 \times P_{CO_2} \exp\left(\frac{-198000}{RT}\right)$ where R is the gas constant and t the time (s). Reaction mechanism is similar to that of the pure iron in analogous conditions, with the same rate limiting step i.e. external reaction of CO$_2$ with wüstite and outward diffusion of ions Fe^{2+} (not limiting). For weight gains $\Delta m/S$ higher than 4 mg cm^{-2}, the limiting step changes, with an increase of the reaction rate and an internal oxidation. The origin of this mechanism change lies in the microcracks appearing in the oxide during its growth. Then, wüstite is no longer bound to the substrate; outward diffusion of ions Fe^{2+} stops and a topotactic transformation converts wüstite into magnetite.

Keywords Invar® · Kinetics · Wüstite · Magnetite · Internal oxidation · Reaction mechanism

Introduction

In the field of thermal plasma deposition, it has been recently shown [1] that the pre-oxidation of steel substrates enhanced the adhesion of ceramic coatings, compared with

S. Menecier · S. Valette · P. Denoirjean · P. Lefort (✉)
SPCTS UMR CNRS 6638, European Ceramic Center,
12 Rue Atlantis, 87068 Limoges, France
e-mail: Pierre.lefort@unilim.fr

the classical method, where the surface of the steel is sandblasted to increase its roughness. This new process is very promising because sandblasting is inadequate for many kinds of pieces (thin, complex…), whereas the pre-oxidation can always be applied. The best results were observed when wüstite Fe$_{1-x}$O is formed [1, 2] according to the reaction:

$$(1 - x)Fe + CO_2 \rightarrow Fe_{1-x}O + CO \tag{1}$$
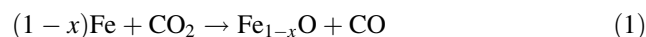
that requires a sample heating in CO/CO$_2$ mixtures or in pure CO$_2$ atmosphere. It was worth verifying if such a process could be applied to Invar®.

This alloy was chosen because of its low thermal expansion coefficient ($\alpha = 1$–10×10^{-6} K^{-1} according to temperature) [3] that limits the thermal stresses at the interface {alloy substrate/ceramic coating} when the temperature changes. Indeed, usual ceramics have thermal expansion coefficients of 2–10×10^{-6} K^{-1}, close to that of the Invar® whereas most of the metals are in the range of 10–20×10^{-6} K^{-1}. Moreover, it has been shown that a surface oxidation of the alloy strongly improves the ceramic/metal bonding, above all because it prevents the gap of physical properties at the interface [1, 4].

Therefore, in order to optimize the thermal plasma deposition of ceramics on Invar®, it was first necessary to focus on the oxidation conditions of this alloy in CO$_2$, using a process that was easy to industrialize, i.e. in the static CO$_2$ of a moderate quality. Now, no article has been devoted to the reaction Invar®/CO$_2$. The reason explaining this is probably the fact that Invar® has very few uses at high temperature and especially in a CO$_2$ atmosphere (even stainless steels are only little studied at high temperature in CO$_2$ [5–7]).

Hence, the present study was necessary to establish the kinetically and morphological conditions required for the

formation of a superficial oxide layer on Invar® substrates, in view of industrial applications. Moreover, it also allowed deepening the fundamental mechanism of this reaction, in particular by comparison with former works on pure iron and steels [1, 5–11].

Experimental

Invar® substrates

The samples of 10 × 10 mm were cut off, from an Invar® sheet 500 μm thick (IMPHY SA, France). Hence, the surface in contact with gas was of 2.2 cm² for an initial mass of 390 ± 10 mg. Table 1 presents the nominal composition of the alloy, the main impurities of which were manganese and silicon. X-ray diffraction (XRD) patterns of the surface identified the only presence of the taenite phase (Fe,Ni) (JCPDS file 23-0297).

Gas

The gases used were industrial carbon dioxide (Air Liquide, France, ONU number 1013 class 2) and argon (Air Products SA, France, Alphagaz Ar 1). Their main impurities were water and oxygen in contents lower than 5 ppm (see Table 2).

Thermogravimetry

Oxidation kinetics were carried out by using a conventional continuous recording balance Setaram B70 with a $MoSi_2$ furnace. A Pt/Pt–Rh (10%) thermocouple was placed under the sample for controlling its temperature. Carbon dioxide partial pressure was adjusted by argon additions for an overall pressure equal to 10^5 Pa and always in a static atmosphere. Before oxidation, Invar® substrates were polished with SiC paper (grade 2400 and 4000 mesh), then cleaned up with ethanol and dried.

For isobaric and isothermal studies, the sample was maintained out of the furnace warm zone during temperature rise. Once the chosen temperature reached, the sample was placed in the middle of the furnace and the acquisition was launched. At the end of the experiment, the sample was quenched in the furnace cold zone, in the same gas atmosphere.

Samples characterization

Phases identifications were performed using an X-ray Brüker D5000 diffractometer equipped with a back monochromator ($\lambda_{Cu} = 0.1541$ nm). The scanned angles (in 2θ scale) ranged between 17 and 90° with a step of 0.015° and a 10 s exposure time. The X-ray patterns were indexed using DIFFRAC+ software (Socabim) containing JCPDS files database. Surface samples were observed by Scanning Electron Microscopy (SEM Philips XL30) equipped with EDS facilities (EDAX®). Transmission electron microscopy study was performed using a Jeol 2010 TEM working at 200 kV.

Results

Kinetics

Figure 1 presents the weight gain ($\Delta m/S$) of an Invar® sample during a linear rise of temperature (5 K min⁻¹). No weight change was seen below approximately 850 K. At higher temperatures, the reaction accelerated slowly before becoming very fast above approximately 1350 K. From this result, it was chosen to study the oxidation between 1163 and 1263 K.

For the longest oxidation times (e.g. for 50 h at 1243 K in Fig. 2), kinetics were sigmoid, and XRD analysis identified magnetite Fe_3O_4 as final product, which means that the overall reaction was

$$3Fe + 4CO_2 \rightarrow Fe_3O_4 + 4CO \qquad (2)$$

without any trace of nickel oxidation. The weight gain observed (ca. 42 mg cm⁻²) corresponds to what was expected, according to reaction (2), by considering that all the iron contained in the alloy was oxidized, for a sample with initial mass of 390 mg.
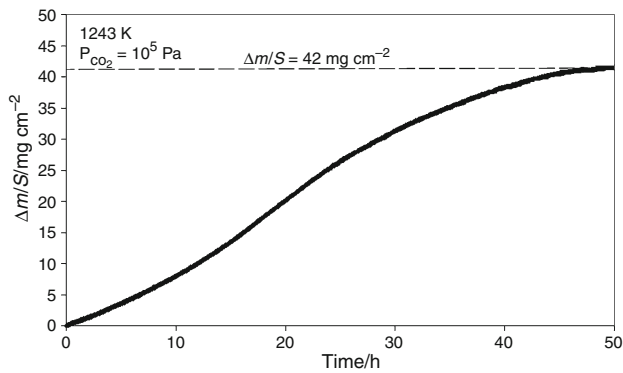
Table 1 Invar® sheet nominal composition

Element	C	Mn	Si	S	P	Ni	Cr	Co	Al	Fe
Wt%	0.0032	0.294	0.096	Traces	<0.002	35.91	0.058	0.059	0.0050	Bal.

Table 2 Main impurities of the gas used

Gas	Argon		CO₂	
Impurities	H₂O	O₂	H₂O	O₂
Content	≤3 ppm	≤2 ppm	≤5 ppm	≤5 ppm
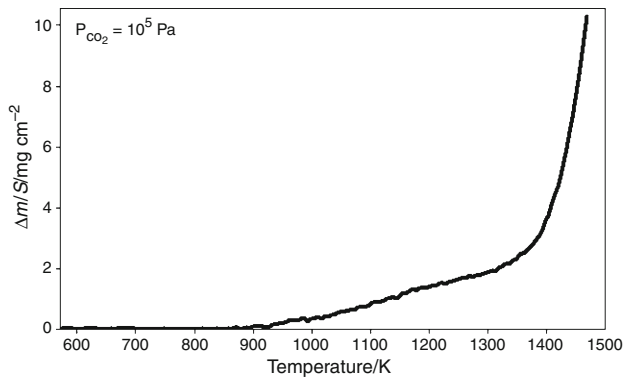
Fig. 1 Oxidation of Invar® in CO_2 during a linear rise of temperature (5 K min^{-1})

Fig. 2 Isotherm at 1243 K for 50 h in 10^5 Pa of CO_2

Fig. 3 Isotherms for 20 h with a CO_2 pressure of 10^5 Pa (a) and isobars at 1243 K in CO_2 atmosphere (b)

Fig. 4 Transformation by an affinity in time of the isotherms (a) and of the isobars (b)

As far as the aim of this study was determining the formation condition of thin bonding layers of oxide at the surface of the alloy and not its complete corrosion, isothermal and isobaric oxidations were limited to their beginning ($\Delta m/S$ <5 mg cm^{-2}).
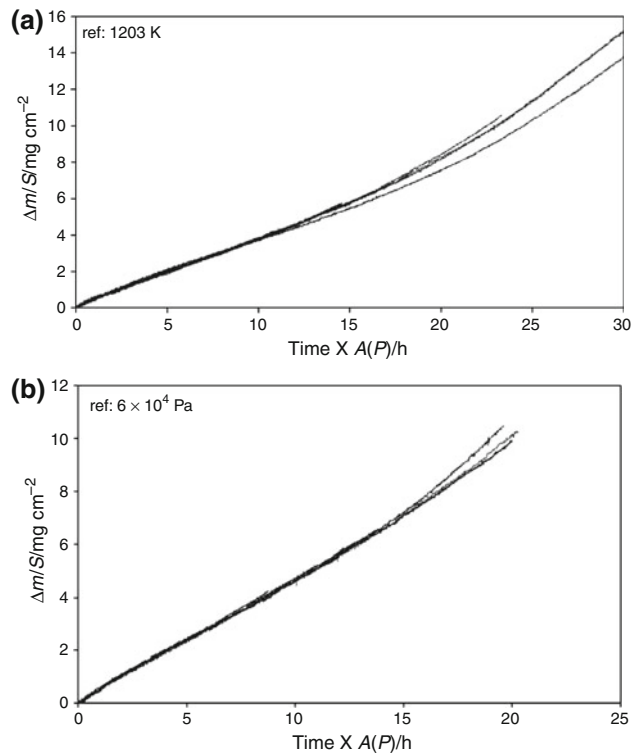
Isotherms in 10^5 Pa of CO_2 and isobars at 1243 K are presented respectively, in Fig. 3a, b. They are quite linear in the range $0.5 < \Delta m/S < 4$ mg cm^{-2}, after a short initial deceleration, and for weight gains higher than 4 mg cm^{-2}, a slight acceleration is perceptible that corresponds to the beginning of the accelerated part seen on the sigmoid curve of Fig. 2.

The curves were analysed using affinity in time [12]. This method consists of multiplying time of each curve by an appropriate coefficient A (A is different for each kinetic) to superimpose them onto one of them, which is considered as the reference. This analytical method offers two main advantages, if the curves superimpose

– it proves that the reaction mechanism is the same for all the considered time;
– it allows determining directly the apparent activation energy and the pressure law without any assumption about the reaction mechanism.
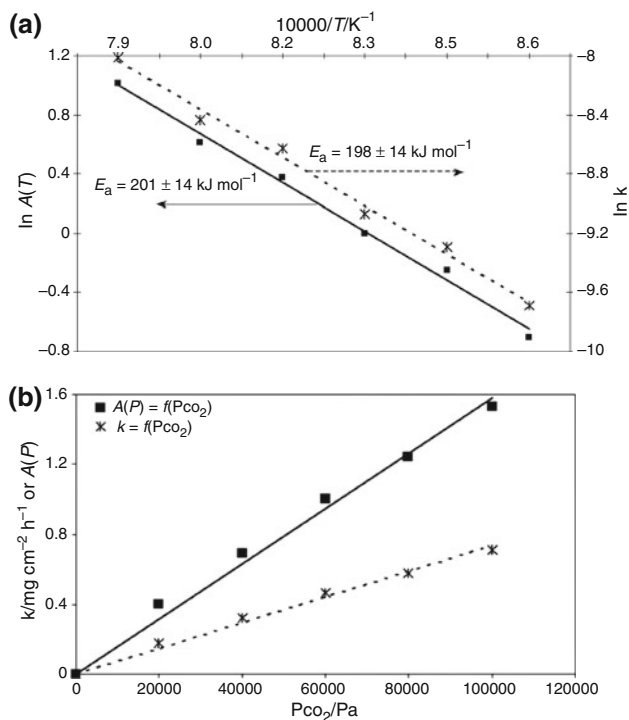
The isotherm for $T = 1203$ K and the isobar for $P_{CO_2} = 6 \times 10^4$ Pa were considered as the references, and Fig. 4a, b show a good superimposition of isotherms and isobars up

Fig. 5 Influence of temperature (**a**) and of CO_2 partial pressure on oxidation kinetic of Invar® (**b**)

Table 3 Phases identified by XRD according to temperature (T), weight gain ($\Delta m/S$) and duration, in 10^5 Pa of CO_2 (P' = wüstite P' phase, P'' = wüstite P'' phase and M = magnetite)

T/K	Phases	$\Delta m/S$/mg cm^{-2}	Time/h
1163	Invar®, P', P''	1.0	4
1163	P', P'', M	4.1	20
1183	Invar®, P', P''	1.5	4
1203	Invar®, P', P''	1.7	4
1223	Invar®, P', P''	2.8	4
1243	P', P''	3.1	4
1263	P', P'', M	4.6	4

to weight gains ca. 4 mg cm^{-2}. For higher weight gains, the curves diverge, which means that the reaction mechanism changed at ca. 4 mg cm^{-2}. For the isotherms, the values of $A(T)$, plotted in Fig. 5a, using Arrhenius coordinates, gave the apparent energy of activation $E_a = 201 \pm 14$ kJ mol^{-1}.

For the isobars, the pressure law could be drawn from the values of affinity coefficients $A(P)$, Fig. 5b showing a linear influence of P_{CO_2}.

These results prove [12] that there was only one reaction mechanism at the beginning, for $\Delta m/S$ <4 mg cm^{-2}.

Considering the linear part of the isotherms, their slopes (k) plotted in Arrhenius coordinates (see Fig. 5a) also gave an apparent activation energy value $E_a = 198 \pm 14$ kJ mol^{-1}, in accordance with the value calculated by the direct method of affinities. For the isobars, the variations of their slopes (k) in the linear part of the kinetics, presented in Fig. 5b, also confirmed the linear influence of CO_2 pressure.

Characterization of the oxides layers

XRD patterns of partially oxidized samples identified wüstite (Fe$_{1-x}$O) as being the only reaction product, from the early beginning up to weight gains of about 4 mg cm^{-2}, whatever temperature or pressure could be. For higher weight gains, magnetite traces (Fe$_3$O$_4$) were detected. Two varieties of wüstite were found: P' wüstite

phase Fe$_{1-x}$O ($0.909 < 1-x < 0.945$, JCPDS file 01-073-2144) with traces of P'' wüstite (Fe$_{0.909}$O, JCPDS file 01-086-2316). Table 3 summarizes the different phases detected according to oxidation duration, temperature, pressure and weight gain.

SEM observations showed that, at the early beginning of the reaction (e.g. 0.4 mg cm^{-2}), the oxide formed coated only partially the sample surface, with scattered germs (Fig. 6a, b), which grew and gathered for a higher mass gain (e.g. 0.7 mg cm^{-2}), with a preferential outward growth (Fig. 6c, d). Then, the entire sample surface was covered (e.g. in Fig. 6e, f for a weight gain of 3.1 mg cm^{-2}), with large wüstite crystals (see Fig. 7a).

Inside the alloy, porosity appeared, and around a weight gain of 4 mg cm^{-2}, a zone of internal oxidation rapidly occured. It became well visible for greater weight gains, as on Fig. 7c. Between this zone and the wüstite, a lot of small pores appeared, while microcracks went through the wüstite layer.

From the same weight gain of 3–4 mg cm^{-2}, some dark spots appeared at the surface of the wüstite crystallites that became progressively entirely strewn with such spots. Figure 7b presents a micrograph of the surface, for a particularly illustrative sample, where oxidation was carried up to $\Delta m/S = 22.5$ mg cm^{-2} (20 h of reaction at 1243 K in 10^5 Pa of CO_2). On the dark areas, observations in back scattered electrons (BSE) mode, determined an iron/oxygen atomic ratio Fe/O = 0.75 corresponding to that of the magnetite Fe$_3$O$_4$.

The precise localization of magnetite was determined by the TEM microanalyses of Fig. 8 carried out on a sample oxidized for 4 h at 1223 K ($\Delta m/S = 3.1$ mg cm^{-2}). In Fig. 8a, the Invar®/oxide interface is brought to the fore by a dotted white line, while selected area electron diffraction (SAED) patterns of Invar® (axis zone [$\bar{1}$ 10]) and wüstite (axis zone [110]) are respectively, given in the left and right corners of the Figure. No magnetite was found at this

Fig. 6 SEM observations of samples surfaces according to the weight gain
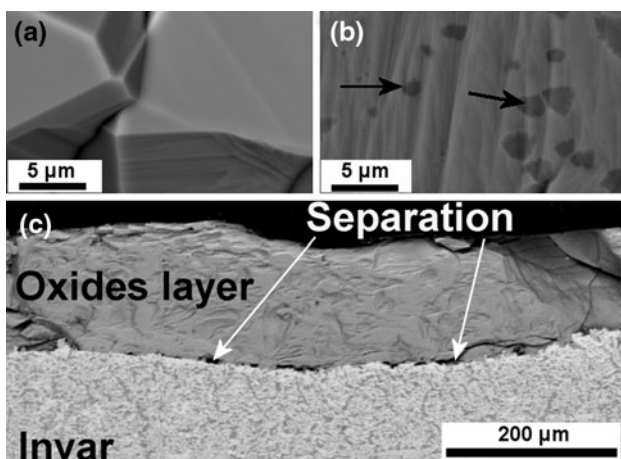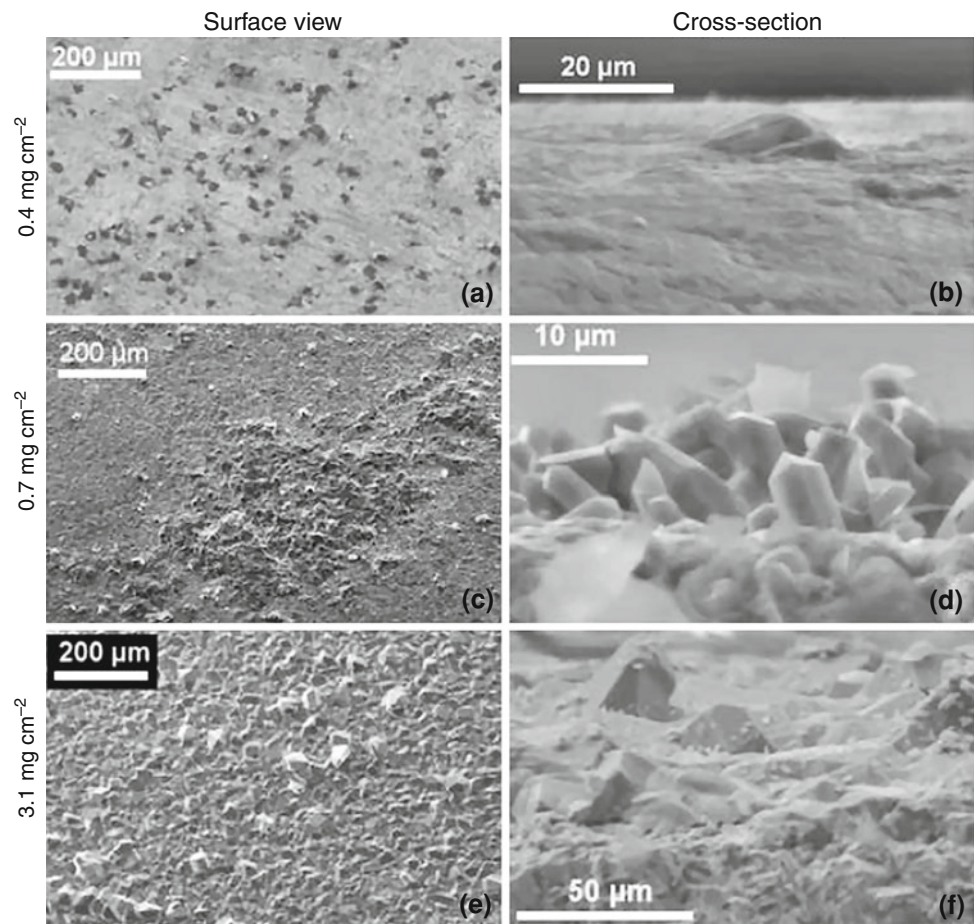
Fig. 7 SEM observations of sample surface after oxidation at 1243 K in 10^5 Pa of CO_2: (a) surface for $\Delta m/S = 3.1$ mg cm^{-2}, (b) surface for $\Delta m/S = 22.5$ mg cm^{-2} and (c) cross section for $\Delta m/S = 32$ mg cm^{-2}

inner interface. On the contrary, at the oxide/gas interface, SAED pattern of Fig. 8b identified both magnetite and wüstite P'' as it can be seen by considering respectively, their [100] and $[\bar{2}\,01]$ axis zones presented on this Figure. This proves that the wüstite → magnetite transformation

took place at the surface of the oxide scale, magnetite being located near the outer interface.

Growth of the oxides layers

In order to clarify the matter transfers during the reaction, a platinum wire was initially welded on an Invar® plate: after a 24 h oxidation at 1243 K under 10^5 Pa of CO_2, the platinum marker was entirely covered by the oxide, which illustrates the outward diffusion of iron, as it can be seen on the cross-section of Fig. 9a.

Figure 9 also provides the corresponding X-ray maps of iron (Fig. 9b), nickel (Fig. 9c) and oxygen (Fig. 9d). They confirm that nickel did not diffuse in the oxide scale. In Fig. 9c nickel keeps the initial thickness of the original Invar® plate, but, near the interface with the oxide, there is a Ni-enriched zone of ca. 120 μm thick, corresponding exactly to a Fe-depleted zone well visible on Fig. 9b. This means that iron went out from this zone to supply the outer oxide formation, while nickel stayed on. Oxygen map of Fig. 9d shows that the internal Fe-depleted zone also contained oxygen, which proves that an internal oxidation occurs in addition to the external growth of the oxide scale.
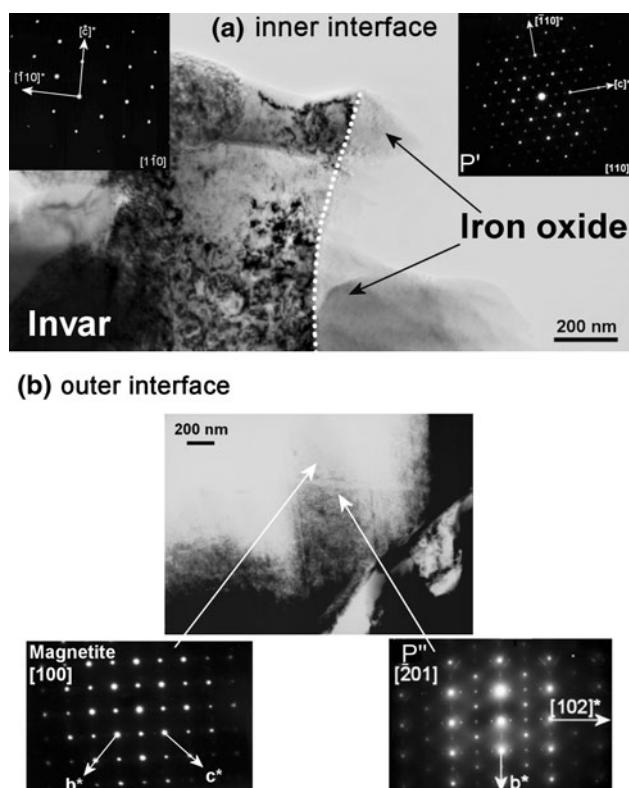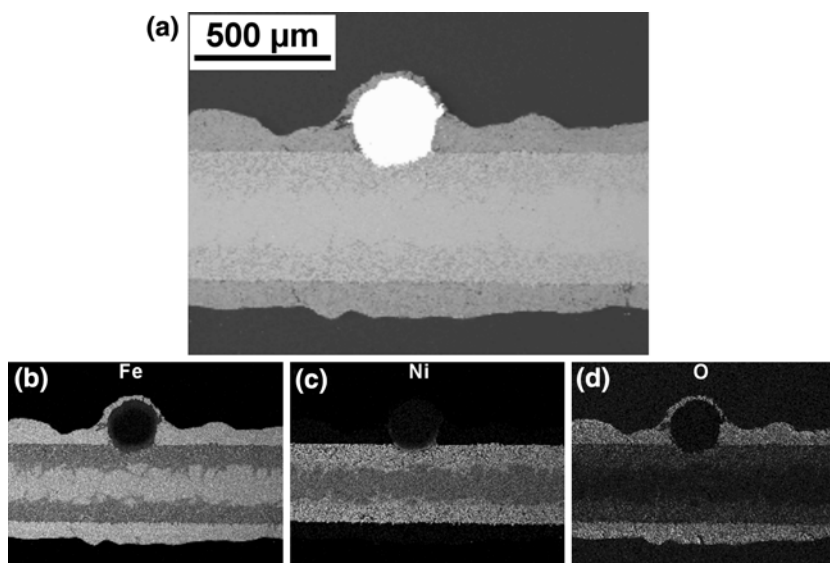
Fig. 8 TEM characterization of Invar® oxidized at 1223 K for 4 h ($\Delta m/S = 3.1$ mg cm^{-2}) in 10^5 Pa of CO_2: (**a**) Inner interface (Invar®/oxide), with the $[1\,\overline{1}\,0]$ axis zone of Invar® SAED pattern (*left corner*) and with the [110] axis zone of wüstite P' SAED pattern (*right corner*), (**b**) Outer interface (oxide/gas), with [100] axis zone of SAED pattern of magnetite (*left*) and with $[\overline{2}\,0\,1]$ axis zone of SAED pattern of P'' wüstite

Discussion

Invar® oxidation in CO_2 leads to the only formation of iron oxides: wüstite and magnetite; no nickel oxide was detected. This is always observed for iron-based alloys oxidized in CO_2, and it is justified by thermodynamical considerations, nickel oxide being reduced by metallic iron.

About the reaction mechanism, for weight gains around 4 mg cm^{-2}, a significant change was pointed out as well by the affinity treatment of the kinetics curves than by morphological observations: kinetics were no longer affine for $\Delta m/S >$ around 4 mg cm^{-2} which means that the reaction mechanism changed above this value. For the same weight gain of 4 mg cm^{-2}, the magnetite phase was quantitatively detected by XRD (Fe_3O_4 has been seen from $\Delta m/S = 3.1$ mg cm^{-2} by TEM, but in too small quantities for its identification by XRD, and for producing any weight effect).

From these elements, it appears that the reaction is composed of two successive steps:

1. formation of wüstite alone, which covers progressively the Invar® surface, and thickens up to $\Delta m/S =$ about 4 mg cm^{-2}. In this part, where kinetics are linear, a kinetic law can be easily carried out;
2. for $\Delta m/S >$ about 4 mg cm^{-2}, wüstite formation goes on, but this oxide also converts into magnetite from the outer interface. Simultaneously, there is an internal oxidation and several morphological changes.

Kinetic law

At the early beginning of the reaction ($\Delta m/S < 0.5$ mg cm^{-2}), germs of wüstite progressively cover the Invar® surface and grow. The so-formed thin layer is probably protective enough for justifying the slight initial kinetics deceleration.

Fig. 9 Cross section of the oxidized sample with platinum marker (**a**) and corresponding X-ray maps of Fe (**b**), Ni (**c**) and O (**d**)

For the following linear part of kinetics ($0.5 < \Delta m/S < 4$ mg cm^{-2}) a simple law can be easily established, corresponding to the thickening of the wüstite layer according to Eq. 1, before magnetite quantitative formation.
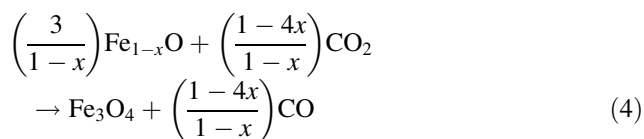
$$(1 - x)\text{Fe} + \text{CO}_2 \rightarrow \text{Fe}_{1-x}\text{O} + \text{CO} \quad (1)$$
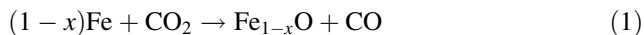
The slopes k of the isotherms and of the isobars of Fig. 3 lead to the rate law:

$$r = \frac{d\left(\frac{\Delta m}{S}\right)}{dt} = 0.41 \times P_{CO_2} \exp\left(\frac{-198000}{RT}\right) \quad (3)$$

where the rate r is expressed in mg cm^{-2} s^{-1}, for $2 \times 10^4 \leq P_{CO_2} \leq \times 10^5$ Pa, $1163 \leq T \leq 1263$ K and $0.5 \leq \Delta m/S \leq 4$ mg cm^{-2}.

For $\Delta m/S > 4$ mg cm^{-2}, Fig. 2 shows that reaction rate increases, and the curves are no longer affine (see Fig. 4a, b). This means that another reaction occurs quantitatively, which has been identified as the formation of magnetite, through Eq. 4 occurring at the same time as reaction (1).

$$\left(\frac{3}{1-x}\right)\text{Fe}_{1-x}\text{O} + \left(\frac{1-4x}{1-x}\right)\text{CO}_2$$
$$\rightarrow \text{Fe}_3\text{O}_4 + \left(\frac{1-4x}{1-x}\right)\text{CO} \quad (4)$$

Concerning the weight effect of these reactions, it is worth noticing that reaction (1) corresponds to a weight gain which is three times greater than that of reaction (4): 32.6 mg cm^{-2} instead of 10.9 mg cm^{-2}.

Otherwise, near the end of the reaction, when iron is quite completely consumed, reaction (4) remains alone, and this explains the slackening observed in Fig. 2 from $\Delta m/S =$ about 27 mg cm^{-2}.

The simultaneity of the two reactions, with weight effects depending on time, and with different localizations, makes impossible the expression of a kinetic law for $\Delta m/S > 4$ mg cm^{-2}.

Nature of the oxides and reaction mechanism

Beginning of the reaction ($\Delta m/S > 4$ mg cm^{-2})

The nature of the oxides has to be examined together with the mechanism proposal, since from a thermodynamical point of view, magnetite should be the only oxide produced, if CO₂ was absolutely pure. Moreover, molecular oxygen and water, present in the gas used (<5 ppm, see Table 2), and mainly the traces of O₂ remaining in the furnace before the introduction of CO₂, favours also the formation of magnetite. Of course, the production of carbon monoxide by reaction (1), could justify apparently the formation of wüstite. But, in fact, even the complete oxidation of a sample produces a quantity of CO (about $6 \times 10^{-3}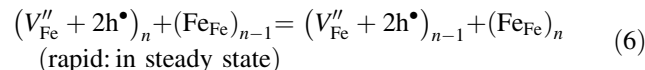$ mol) related to the amount of CO₂ in the recording balance (approximately 0.35 mol), lower than that is required for the stabilization of the wüstite, as previously established on the basis of thermodynamical tables [9, 13, 14]: for instance, at 1200 K the ratio log P_{CO}/P_{CO_2} (−1.77) remains much lower than the value thermodynamically required for the formation of wüstite (−0.278). Clearly, P_{CO} is always too low for stabilizing wüstite (Fe$_{1-x}$O), and even if Fe₃O₄ is actually the final product, the intermediate formation of wüstite has to be explained.

Several authors such as Smeltzer et al. [8, 9] or Kofstad et al. [15–17] have already pointed out this question, but in experimental conditions that were somewhat different from those of the present study, since the substrates were pure iron and the reactive atmospheres were generally composed of CO/CO₂ mixtures. Nevertheless, the similarity of kinetics and of the reaction products leads to examine their conclusions. Kofstad claims that wüstite forms, according to the following surface elementary reaction (limiting step):
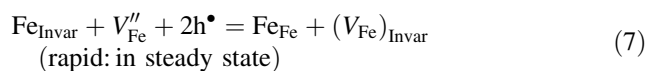
$$\text{CO}_{2[g]} \rightarrow \text{O}_\text{O} + V_\text{Fe}'' + 2\text{h}^\bullet + \text{CO}_{[g]} \quad \text{(slow)} \quad (5)$$
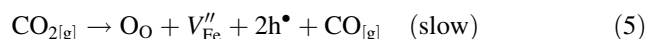
using the Kröger-Vink notation [18], where O_O, V_Fe'' and h$^\bullet$ represent respectively, an oxygen anion in the wüstite lattice, a Fe^{2+} vacancy and an electron hole.

In this equation, if so, vacancies V_Fe'' and electron holes h$^\bullet$ appearing at the outer interface necessarily diffuse inwards, corresponding to an outward flow of iron ions Fe^{2+} such as:

$$\left(V_\text{Fe}'' + 2\text{h}^\bullet\right)_n + (\text{Fe}_\text{Fe})_{n-1} = \left(V_\text{Fe}'' + 2\text{h}^\bullet\right)_{n-1} + (\text{Fe}_\text{Fe})_n$$
$$\text{(rapid: in steady state)} \quad (6)$$

where the index n represents the level of the oxide crystalline plane considered ($n = 0$ on the Invar®/oxide interface and n is maximum at the interface oxide/gas). In the present study, this outward iron diffusion has really been confirmed by the platinum marker test of Fig. 9.

Figures 10a, b schematise respectively the elementary reaction on the surface (5) and the diffusion step (6). At the inner interface, metallic iron meets vacancies V_Fe'' and holes h$^\bullet$, and it reacts with them by:

$$\text{Fe}_\text{Invar} + V_\text{Fe}'' + 2\text{h}^\bullet = \text{Fe}_\text{Fe} + (V_\text{Fe})_\text{Invar}$$
$$\text{(rapid: in steady state)} \quad (7)$$

with formation of an iron atom vacancy $(V_\text{Fe})_\text{Invar}$ in the alloy and a Fe^{2+} cation Fe$_\text{Fe}$ in the wüstite lattice (Fig. 10c).

This proposal of limiting step (Eq. 5) is in good agreement with the kinetics linearity observed here, since the reactive area (i.e. the place where the limiting step is located) is the external surface of the oxide: this area remaining constant with time, reaction rate also remains constant.

It can also justify why wüstite forms instead of magnetite: as soon as one oxygen anion is captured at the

**Fig. 10** Elementary steps of Invar® oxidation (beginning)
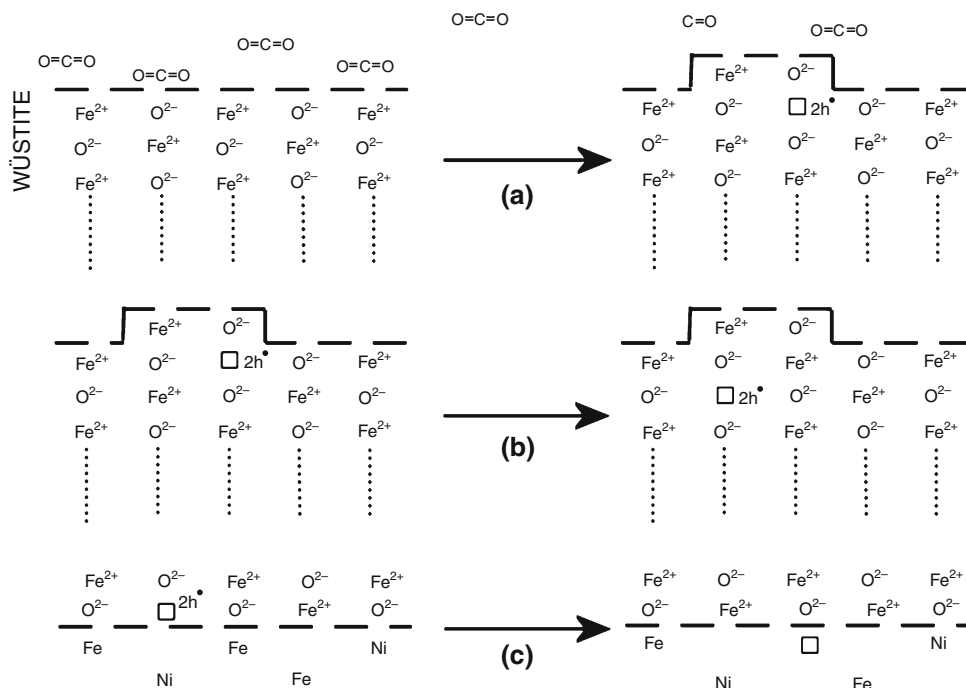
surface of the oxide (Eq. 5), step slow, accompanied by the creation of a vacancy V''_{Fe}), one ion Fe^{2+} arrives immediately at the surface and fills the vacancy V''_{Fe} (Eq. 6, step rapid), so that the defect $(V''_{Fe}, 2h^{\bullet})$ never stays at the surface of the outer crystals. Indeed, one may consider that the topotactic transformation of wüstite (fcc structure) into magnetite (spinel structure) is the consequence of the accumulation of defects $(V''_{Fe}, 2h^{\bullet})$ inside the wüstite structure, by:

$$2Fe_{Fe} + V''_{Fe} + 2h^{\bullet} = 2Fe^{\bullet}_{Fe} + V''_{Fe} \qquad (8)$$
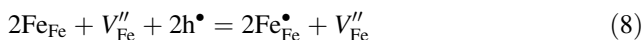
where $Fe^{\bullet}_{Fe}$ represents a former ion Fe^{2+} converted into an ion Fe^{3+}: the inward flow of defects $(V''_{Fe}, 2h^{\bullet})$ is probably so rapid through Eq. (6) that the topotactic transformation has not enough time to occur.

This mechanism is summarized in the schematic cross section of Fig. 11, which gives the relative content of metallic iron [Fe] (alloy side) and that of vacancies $[V''_{Fe}]$ (oxide side). Going from the core of the alloy (at the left) towards the surface (at the right) are

- The alloy, where the iron concentration is the nominal one of Invar® (about 64 mol %);
- Near the interface alloy/oxide, a zone where the iron content is very low (as seen in Fig. 9b) since this element is pulled out from the alloy and goes outwards;
- The oxide, where the vacancies content is that of wüstite (around 5–9 mol %) and remains constant because their diffusion is not the limiting step;
- Finally, the limiting reaction, on the surface (Eq. 5).
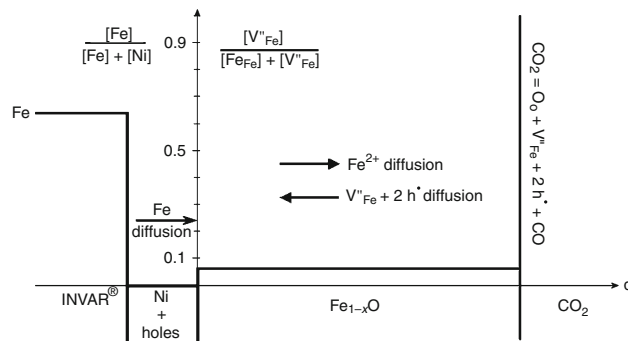
Fig. 11 Relative contents of iron in the substrate and of vacancies V''_{Fe} in wüstite, represented in cross section, with the limiting step located at the outer interface ($\Delta m/S < 4$ mg cm^{-2})

Weight gains higher than 4 mg cm^{-2} (sigmoid part)

For $\Delta m/S > 4$ mg cm^{-2} the mechanism presented above has to be modified to explain why the internal oxidation occurs and why magnetite appears.

One hypothesis could be that oxygen diffuses at the opposite of iron through the wüstite layer, from the surface to the substrate, and finally reacts with the iron of Invar®. However, this has never been reported in the literature, and the difference between the self-diffusion coefficients of iron ($D_{Fe} = 7.8 \times 10^{-12}$ m^2 s^{-1}, calculated from [19]) and oxygen ($D_O = 2 \times 10^{-17}$ m^2 s^{-1} [20]) makes this hypothesis very unlikely.

Fig. 12 Oxidation mechanisms for weight gains lower (**a**) and greater (**b**) than 4 mg cm^{-2}

(**a**) $\Delta m/S < 4$ mg cm^{-2}

CO_2

$(1-x)$ Fe + CO_2 = $Fe_{(1-x)}$O + CO

$Fe_{(1-x)}$O

Fe

invar

(**b**) $\Delta m/S > 4$ mg cm^{-2}

3 $Fe_{(1-x)}$O + $(1-4x)$ CO_2 = $(1-x)$ Fe_3O_4 + $(1-4x)$ CO

$(1-x)$ Fe + CO_2 = $Fe_{(1-x)}$O + CO

Internal oxidation zone

Fe

Fe
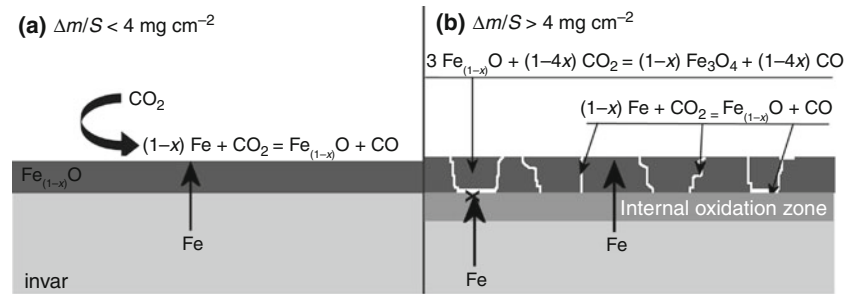
Another hypothesis is that the iron vacancies produced by Eq. 7 gather at the alloy/oxide interface, forming the holes seen on Fig. 7c. Indeed, it is probable that diffusion of Fe in the alloy is slower than the diffusion of Fe^{2+} in the wüstite (Fe is bigger than Fe^{2+}, but no data is available about the auto diffusion of iron in Fe–Ni alloys). Hence, the progressive formation of the holes observed may result in the reduction of the surface contact alloy/oxide, and finally limit the iron diffusion outwards and weaken the bonding substrate/oxide.

The appearance of a network of micro-cracks inside the wüstite layer is probably a consequence of this, joined to the fact that strong stresses appear in the oxide layer during its thickening, as already mentioned previously [21, 22], because of the high value of the Pilling and Bedworth Ratio (*PBR*) of wüstite Fe_{1-x}O formed from Invar®, equal to 2.7.

These two phenomena (formation of holes at the interface oxide/metal and cracks into the oxide scale) can easily justify the direct access of CO_2 to the substrate leading to the internal oxidation of the alloy, seen in the porosity of the substrate.

Finally, when the wüstite layer is no longer bonded to the alloy, iron cannot diffuse anymore towards the wüstite surface, and then the topotactic transformation of wüstite in magnetite (Eq. 8) can begin, forming so the final oxide, forecast by thermodynamic.

Figure 12 allows comparing the reaction mechanism before the cracking of the wüstite layer (Fig. 12a) and after (Fig. 12b).

This last hypothesis has to be accepted because it explains both the internal oxidation and the change of reaction mechanism for weight gains $\Delta m/S > 4$ mg cm^{-2}, the origin of which lies in a mechanical stress relaxation at the interface wüstite/alloy, made brittle by the accumulation of vacancies in this zone. Thus, it provides a consistent explanation for the sigmoidal shape of the kinetics, due to the microstructural changes of the substrate and of the oxide, that induces a change in the nature and in the localization of the reactions: the addition of reactions (4) and (1), joined to the creation of new reactive surfaces inside the porosity of the substrate, led to an acceleration of the weight gain, the final slackening being explained by the depletion in iron of the substrate.

Conclusions

This study presents the oxidation kinetics of Invar® in CO_2 at $1163 \leq T \leq 1283$ K and $2 \times 10^4 \leq P_{CO_2} \leq \times 10^5$ Pa. Characterization of the reaction products shows the only formation of wüstite with an outward diffusion of ions Fe^{2+}, up to a mass gain of about 4 mg cm^{-2}, associated to the linear part of the kinetics. The corresponding apparent energy of activation is of 198 ± 14 kJ mol^{-1}, while the rate depends linearly on the pressure of CO_2. The overall reaction is then governed by the external elementary reaction of CO_2 with wüstite.

If the oxidation continues, for weight increases higher than 4 mg cm^{-2}, a mechanical relaxation of stresses at the interface oxide/alloy leads a mechanism change, with penetration of CO_2 through the oxide scale, which gives an internal oxidation. Consequently, the outward diffusion of ions Fe^{2+} through the wüstite layer is stopped in the places where oxide and alloy are no longer in contact, and, progressively, wüstite converts into magnetite via a topotactic transformation. As far as the wüstite formation continues inside the alloy, these two simultaneous reactions lead to an increase of the overall reaction rate. Close to the end of the reaction, the rate finally decreases because of the iron depletion, and all this justifies the sigmoidal shape of the overall kinetics.

From a practical point of view, since the plasma deposition of ceramic onto metallic substrates is favoured by the presence of a wüstite layer strongly bonded to the substrate, in the case of Invar® the preheating step must be carefully processed to obtain wüstite alone and having a controlled thickness rather thin, i.e. before the appearance of the first micro-cracks.

References

1. Valette S, Trolliard G, Denoirjean A, Lefort P. Iron/wüstite/magnetite/alumina relationships in plasma coated steel: a TEM study. Solid State Ionics. 2007;178:429–37.
2. Valette S, Denoirjean A, Lefort P, Fauchais P. Influence of dc plasma preheating on oxide layers formed by furnace heating on low carbon steel substrates and resulting adhesion/cohesion of alumina coatings. High Temp Mater Process. 2003;7:205–15.

3. Inaba M, Honma Y, Hatanaka T, Otake Y. Effects of the annealing conditions on the oxidation behavior of Fe-36 Ni alloys. Appl Surf Sci. 1986;27:164–79.

4. Zanchetta A, Gabbay E, Lefort P. Thermal expansion and adhesion of ceramic to metal sealings: case of porcelain-kovar junctions. J Eur Ceram Soc. 1995;15:233–8.

5. Vourlias G, Pistofidis N, Pavlidou E, Chrissafis K. Oxidation behaviour of precipitation hardened steel TG, X-ray, XRD and SEM study. J Therm Anal Calorim. 2009;95:63–8.

6. Lauretta DA, Schmidt BE. Oxidation of minor elements from an iron–nickel–chromium–cobalt–phosphorus alloy in 17.3% CO_2–H_2 gas mixtures at 700–1000 °C. Oxid Met. 2009;71:219–35.

7. Goutier F, Valette S, Vardelle A, Lefort P. Oxidation of stainless steel 304L in carbon dioxide. Corr Sci. 2010;52:2403–12.

8. Smeltzer WW. Kinetics of wüstite scale formation on iron. Acta Metall Mater. 1960;8:377–83.

9. Smeltzer WW, Morris LA, Logani RC. Growth of wüstite scales on steels. Can Metall Quart. 1970;9:513–9.

10. Pettit F, Yinger R, Wagner JB. The mechanism of oxidation of iron in carbon monoxide-carbon dioxide mixtures. Acta Metall Mater. 1960;8:617–23.

11. Valette S, Denoirjean A, Tétard D, Lefort P. C40E steel oxidation under CO_2: kinetics and reactional mechanism. J Alloy Compd. 2006;413:222–31.

12. Barret P. Cinétique Hétérogène. Paris: Gauthier-Villars; 1973.

13. Valette S, Ménecier S, Goutier F, Lefort P. Kinetics of some iron-based alloys in industrial CO_2: formation of wüstite phase. Mater Sci Forum. 2008;595–598:1153–61.

14. Barin I, Knacke O. Thermochemical properties of inorganic substances. Düsseldorf: Springer-Verlag; 1973.

15. Bredesen R, Kofstad P. On the oxidation of iron in CO_2+CO gas mixtures: I. Scale morphology and reaction kinetics. Oxid Met. 1990;34:361–79.

16. Bredesen R, Kofstad P. On the oxidation of iron in CO_2+CO mixtures: II. reaction mechanisms during initial oxidation. Oxid Met. 1991;35:107–37.

17. Bredesen R, Kofstad P. On the oxidation of iron in CO_2+CO mixtures. III: coupled linear parabolic kinetics. Oxid Met. 1991;36:27–56.

18. Kröger FA, Vink HJ. Relations between the concentrations of imperfections in crystal solids. In: Seitz F, Turnbull D, editors. Solid State Physics, vol. 3. New York: Academic; 1956. p. 307–435.

19. Chen RY, Yuen WYD. Oxidation of low-carbon steel in $17H_2O$–N_2 at 900 °C. Metall Mater Trans A. 2009;40:3091–107.

20. Yamaguchi S, Someno M. The tracer diffusivity of oxygen in wüstite and cobaltous oxide. Trans Jpn Inst Met. 1982;23:259–66.

21. Mitchell TE, Voss DA, Butler EP. The observation of stress effects during the high temperature oxidation of iron. J Mater Sci. 1982;17:1825–33.

22. Perusin S. Conséquences de l'oxydation haute température sur l'injection de défauts et le comportement mécanique des matériaux métalliques. PhD thesis; CIRIMAT: Toulouse; 2004.